Remnants of the Early Solar System Water Enriched in Heavy Oxygen Isotopes

Naoya Sakamoto,[1] Yusuke Seto,[1] Shoichi Itoh,[1] Kiyoshi Kuramoto,[2] Kiyoshi Fujino,[1] Kazuhide Nagashima,[3] Alexander N. Krot,[3] Hisayoshi Yurimoto[1,4]*

Oxygen isotopic composition of our solar system is believed to have resulted from mixing of two isotopically distinct nebular reservoirs, ^{16}O-rich and ^{17,18}O-rich relative to Earth. The nature and composition of the ^{17,18}O-rich reservoir are poorly constrained. We report an in situ discovery of a chemically and isotopically unique material distributed ubiquitously in fine-grained matrix of a primitive carbonaceous chondrite Acfer 094. This material formed by oxidation of Fe,Ni-metal and sulfides by water either in the solar nebula or on a planetesimal. Oxygen isotopic composition of this material indicates that the water was highly enriched in ^{17}O and ^{18}O ($\delta^{17,18}O_{SMOW}$ = +180‰ per mil), providing the first evidence for an extremely ^{17,18}O-rich reservoir in the early solar system.

Oxygen isotopic variations in chondrites provide important constraints on the origin and early evolution of the solar system (*1*). Oxygen isotope ratios in chondrites change not only by mass-dependent isotope fractionation law (isotope fractionation depending on mass differences among isotopes) but also by large mass-independent isotope fractionation (MIF) that keeps ^{17}O/^{18}O ratio nearly constant. It is generally accepted that MIF recorded by meteorites resulted from mixing of two isotopically distinct nebular reservoirs, ^{16}O-rich and ^{17,18}O-rich (*2*). The composition of the ^{16}O-rich reservoir has been recently constrained from isotopic compositions of nebular condensates (*3*) and of a unique chondrule (*4*). The nature and composition of an ^{17,18}O-rich nebular reservoir are still poorly constrained (*5*, *6*). According to the currently favorite self-shielding models (*7*–*11*), nebular water is hypothesized to have been highly enriched in ^{17,18}O (5 to 20%) relative to Earth, which is, however, yet to be verified by isotope measurements. Here we report an in situ discovery of a chemically and isotopically unique material in the primitive carbonaceous chondrite Acfer 094. This material is mainly composed of iron, oxygen, and sulfur, and is highly enriched in ^{17}O and ^{18}O (up to +18%) relative to Earth's ocean. Mineralogical observations and thermodynamic analysis suggest that this material resulted from oxidation of iron metal and/or iron sulfide by water in the solar nebula or on a planetesimal. We infer that the extreme oxygen isotopic composition of this material recorded composition of this primordial water that corresponds to an ^{17,18}O-rich nebular reservoir in the early solar system, in agreement with the self-shielding models (*7*–*12*).

During our ongoing in situ survey (*13*–*16*) of presolar grains of primitive meteorites (*17*), we discovered isotopically anomalous regions of oxygen in matrix of the ungrouped carbonaceous chondrite Acfer 094 in addition to isotopically anomalous spots corresponding to presolar grains (Fig. 1). The oxygen isotopic compositions of the regions are uniform and enriched in ^{17}O and ^{18}O relative to ^{16}O (Fig. 2). The data seem to be plotted along the slope-1 line (*18*) rather than the carbonaceous chondrite anhydrous mineral mixing (CCAM) line (*2*) (Fig. 3). The representative values of $\delta^{17}O_{SMOW} = \delta^{18}O_{SMOW}$ are about +180 per mil (‰); SMOW is standard mean ocean water (*19*). These are the heaviest oxygen isotopic compositions of the solar system materials reported so far. The less ^{17}O- and ^{18}O-rich compositions ($\delta^{17,18}O_{SMOW}$ = +50‰) of unknown origin have been recently reported in the surface layers of metal grains from lunar regolith (*20*).

The chemical compositions of the isotopically anomalous regions determined by an energy-dispersive x-ray spectrometer (EDS) attached to a field-emission scanning electron microscope (FE-SEM) (*16*) show that they are homogeneous and mainly composed of Fe, Ni, O and S (representatively, in weight percent, Fe, 61.6; Ni, 5.4; O, 19.3; S, 9.6; Mg, 0.1; Si, 0.2). In addition, analytical transmission electron microscopy (ATEM) (*16*) reveals that the regions consist of aggregates of nanocrystals with a size range of 10 to 200 nm (fig. S1). The electron diffraction patterns from ~100-nm-sized individual crystals show that the main spots of the crystals are similar to those of magnetite (Fe_3O_4; space group *Fd3m*); the corresponding cell parameter *a* is 0.83 nm. In addition, there are weak extra spots suggesting a threefold superstructure. Characteristic x-ray spectra from individual crystals show that they consist of the same elements determined by the FE-SEM-EDS study. These observations indicate that the crystals have a magnetite-like structure and may represent a new Fe-O-S–bearing mineral; more detailed characterization is necessary to identify it. Although this mineral consists of the same elements as a poorly characterized phase (PCP) commonly observed in aqueously altered CM chondrites and largely composed of tochilinite or tochilinite-cronstedtite intergrowths (*21*, *22*), its O/S atom ratios are about 4 times as large as those in tochilinite. Hereafter, we refer to this mineral as a new-PCP.

The chemically unique and isotopically anomalous new-PCPs are ubiquitous and scattered randomly throughout the Acfer 094 matrix. Twenty-two new-PCPs (the largest is 160 μm^2) were identified in about an 11-mm^2 area of the matrix using elemental mapping with a 7-μm^2 spatial resolution. This corresponds to 94 ± 20 (σ) parts per million (ppm) by volume. Because the number of the new-PCP grains increases exponentially with decreasing size, the grain numbers below 7 μm^2 are dominant and the actual abundance of new-PCP must be larger than the estimate.

The new-PCP often coexists with troilite (FeS) (Fig. 2), which is considered to be a reaction product between Fe, Ni-metal and H_2S gas (*23*, *24*).

$$Fe + H_2S = FeS + H_2 \quad (1)$$

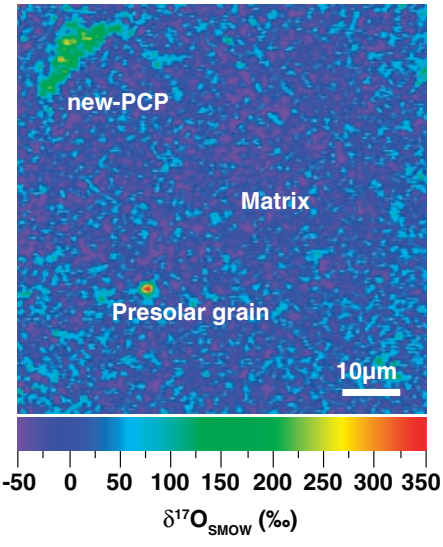

Fig. 1. Spatial distribution of ^{17}O/^{16}O in matrix of the ungrouped carbonaceous chondrite Acfer 094 measured with isotopography (*16*). An isotopically anomalous 10 μm-sized region ($\delta^{17}O_{SMOW}$ = +180‰) and a spot ($\delta^{17}O_{SMOW}$ = +400‰) are surrounded by the isotopically normal matrix materials. The spot corresponds to a presolar silicate grain, whereas the isotopically anomalous region corresponds to a new-PCP.

[1]Department of Natural History Sciences, Hokkaido University, Sapporo 060-0810, Japan. [2]Department of Cosmosciences, Hokkaido University, Sapporo 060-0810, Japan. [3]Hawai'i Institute of Geophysics and Planetology, School of Ocean and Earth Science and Technology, University of Hawai'i at Manoa, Honolulu, HI 96822, USA. [4]Isotope Imaging Laboratory, Creative Research Initiative "Sousei," Hokkaido University, Sapporo, 001-0021, Japan.

*To whom correspondence should be addressed. E-mail: yuri@ep.sci.hokudai.ac.jp

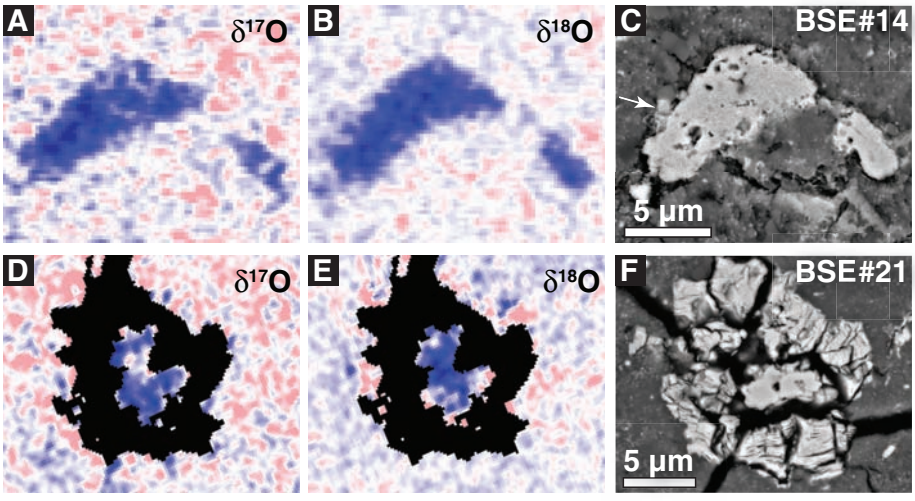

Fig. 2. Oxygen isotopic distribution and grain shape for new-PCP embedded in chondrite matrix. $\delta^{17}O_{SMOW}$ (**A** and **D**), $\delta^{18}O_{SMOW}$ (**B** and **E**), and backscattered electron (**C** and **F**) images for new-PCP #14 [(A) to (C)] and #21 [(D) to (F)] in the Acfer 094 matrix. Arrow in (A) indicates small troilite grains attached to the new-PCP #14. The new-PCP #21 is surrounded by troilite. Because troilite contains no oxygen, the troilite area in (D) and (E) is masked by black color. The new-PCPs are highly enriched in ^{17}O and ^{18}O isotopes relative to the matrix.

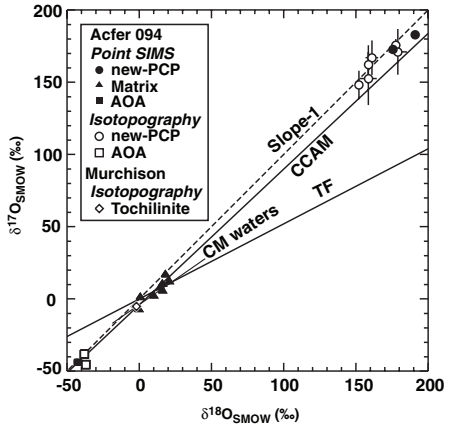

Fig. 3. Oxygen isotopic compositions of the new-PCP from the Acfer 094 matrix. Oxygen isotopic compositions of matrix and amoeboid olivine aggregate (AOA) from Acfer 094 and tochilinite from Murchison are also plotted. The new-PCPs are plotted on extrapolation of slope-1 line or carbonaceous chondrite anhydrous mineral mixing (CCAM) line. The compositions of the Murchison tochilinite are plotted near the terrestrial fractionation (TF) line, along an aqueous alternation line [CM waters (*26*)]. Isotopography: analyzed by precise isotopic imaging with an isotope microscope (*16*). Point SIMS: analyzed by conventional point analysis by secondary ion mass spectrometry (*16*). The data are listed in table S1.

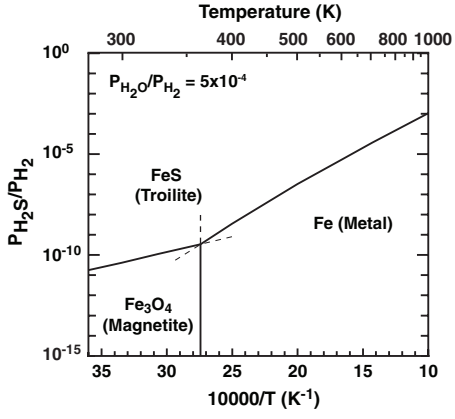

Fig. 4. Calculated equilibrium temperatures for Fe-metal, troilite (FeS) and magnetite (Fe_3O_4) as a function of P_{H2S}/P_{H2} ratio. The magnetite phase boundary is calculated assuming canonical solar nebular H_2O/H_2 ratio of 5×10^{-4} (*30*). Magnetite is considered as a proxy of a new-PCP. Thermodynamic data from JANAF tables (*31*) were used for calculations.

Because new-PCP has magnetite-like diffraction patterns, magnetite can be used as its proxy. Magnetite can be formed by oxidation of Fe, Ni-metal (*23*, *25*), or troilite.

$$3Fe + 4H_2O = Fe_3O_4 + 4H_2 \qquad (2)$$

$$3FeS + 4H_2O = Fe_3O_4 + 3H_2S + H_2 \qquad (3)$$

Oxidation of troilite or metal to form new-PCP would occur below 360 K, independent of total pressure of the solar nebula (Fig. 4). If the nebular P_{H2O}/P_{H2} ratio increases from a characteristic value for a gas of solar composition (*25*), formation of new-PCP occurs at higher temperature. Although the complete chemical equilibrium would not be expected in the cool solar nebula (*23*), the new-PCP would be formed inside the water sublimation front (snowline) of the solar nebula, because water vapor is the major oxidant in the solar nebula and the sublimation temperature of water ice is below 200K even in the several-fold H_2O-enriched nebula (*23*).

Alternatively, new-PCP may have been formed by aqueous alteration of metal and troilite on the Acfer 094 parent body, like tochilinite in the aqueously altered CM chondrites (*22*). To test this hypothesis, we analyzed oxygen isotopic compositions of tochilinite in the CM chondrite Murchison. In contrast to the Acfer 094 new-PCP, oxygen isotopic composition of the Murchison tochilinite is plotted near the terrestrial fractionation line, along the "CM waters" line (*26*) (Fig. 3), that is considered to be a reaction path between aqueous solution and matrix silicates toward the isotope equilibrium (*26*). These observations and the lack of mineralogical and petrographical evidence of aqueous alteration of Acfer 094 (*27*) exclude formation of new-PCP by the aqueous alteration previously observed in chondrites. If new-PCP resulted from oxidation of troilite or metal in a planetesimal setting, a plausible oxidant would be water vapor or aqueous solution that originated from accreted nebular ice and did not experience oxygen isotope exchange with the matrix silicates. In contrast, the inferred oxygen isotopic compositions (*26*, *28*) and the observed chondrite parent body water composition richest in $^{17,18}O$ (*29*) may have recorded equilibration of aqueous solutions with the chondrite matrix silicates.

We conclude that oxygen isotopic compositions of new-PCP in Acfer 094 represent composition of the primordial water of the solar system and the previously hypothesized ^{17}O- and ^{18}O-rich reservoir in the early solar system. The wide oxygen isotopic variations of at least $-80‰ < \delta^{17,18}O < +180‰$ found from hot and cold origin materials must provide new guidelines for the origin of oxygen isotope anomalies in the solar system.

References and Notes

1. R. N. Clayton, *Science* **313**, 1743 (2006).
2. R. N. Clayton, *Annu. Rev. Earth Planet. Sci.* **21**, 115 (1993).
3. A. N. Krot, K. D. McKeegan, L. A. Leshin, G. J. MacPherson, E. R. D. Scott, *Science* **295**, 1051 (2002).
4. S. Kobayashi, H. Imai, H. Yurimoto, *Geochem. J.* **37**, 663 (2003).
5. H. Yurimoto, M. Ito, H. Nagasawa, *Science* **282**, 1874 (1998).
6. A. N. Krot *et al.*, *Astrophys. J.* **622**, 1333 (2005).
7. R. N. Clayton, *Nature* **415**, 860 (2002).
8. H. Yurimoto, K. Kuramoto, *Meteorit. Planet. Sci.* **37**, A153 (2002).
9. H. Yurimoto, K. Kuramoto, *Science* **305**, 1763 (2004).
10. J. R. Lyons, E. D. Young, *Nature* **435**, 317 (2005).
11. H. Yurimoto *et al.*, in *Protostars and Planets V*, B. Reipurth, D. Jewitt, K. Keil, Eds. (Univ. of Arizona Press, Tucson, AZ, 2007) pp. 849–862.
12. E. D. Young, *Lunar Planet. Sci.* **XXXVII**, abstr. no. 1790 (2006).
13. H. Yurimoto, K. Nagashima, T. Kunihiro, *Appl. Surf. Sci.* **203-204**, 793 (2003).
14. S. Itoh, H. Yurimoto, *Nature* **423**, 728 (2003).

15. T. Kunihiro, K. Nagashima, H. Yurimoto, *Geochim. Cosmochim. Acta* **69**, 763 (2005).
16. Materials and methods are available as supporting material on *Science* Online.
17. K. Nagashima, A. N. Krot, H. Yurimoto, *Nature* **428**, 921 (2004).
18. E. D. Young, S. S. Russell, *Science* **282**, 452 (1998).
19. $\delta^{i}O_{SMOW}$ (‰) ≡ $[(^{i}O/^{16}O)_{sample}/(^{i}O/^{16}O)_{SMOW} - 1] \times 1000$, where $i = 17$ or 18.
20. T. R. Ireland, P. Holden, M. D. Norman, J. Clarke, *Nature* **440**, 776 (2006).
21. L. H. Fuchs, E. Olsen, K. J. Jensen, *Smithson. Contrib. Earth Sci.* **10**, 1 (1973).
22. K. Tomeoka, P. R. Buseck, *Geochim. Cosmochim. Acta* **49**, 2149 (1985).
23. B. Fegley Jr., *Space Sci. Rev.* **92**, 177 (2000).
24. D. S. Lauretta, D. T. Kremser, B. Fegley Jr., *Icarus* **122**, 288 (1996).
25. Y. Hong, B. Fegley Jr., *Meteorit. Planet. Sci.* **33**, 1101 (1997).
26. R. N. Clayton, T. K. Mayeda, *Geochim. Cosmochim. Acta* **63**, 2089 (1999).
27. A. Greshake, *Geochim. Cosmochim. Acta* **61**, 437 (1997).
28. E. D. Young, *Philos. Trans. R. Soc. London A* **359**, 2095 (2001).
29. B.-G. Choi, K. D. McKeegan, A. N. Krot, J. T. Wasson, *Nature* **392**, 577 (1998).
30. A. N. Krot, B. Fegley Jr., K. Lodders, H. Palme, in *Protostars and Planets IV*, V. Mannings, A. P. Boss, S. S. Russell, Eds. (Univ. of Arizona Press, Tucson, AZ, 2000) pp. 1019–1054.
31. J. M. W. Chase, *NIST-JANAF Thermochemical Tables, Fourth edition, Journal of Physical and Chemical Reference Data, Monograph 9, Parts I and II* (American Institute of Physics, New York, 1998).

32. We thank Y. Matsuhisa for providing a magnetite standard, T. Kaito and I. Nakatani for assistance with focused ion beam sample preparation, K. Tomeoka for indicating Murchison tochilinite, and E. D. Scott and G. R. Huss for discussion. This work was partly supported by Monkasho (H.Y.) and NASA (A.N.K.).

Supporting Online Material

www.sciencemag.org/cgi/content/full/1142021/DC1
Materials and Methods
Fig. S1
Tables S1 and S2
References

2 March 2007; accepted 17 May 2007
Published online 14 June 2007;
10.1126/science.1142021
Include this information when citing this paper.

How Much More Rain Will Global Warming Bring?

Frank J. Wentz,* Lucrezia Ricciardulli, Kyle Hilburn, Carl Mears

Climate models and satellite observations both indicate that the total amount of water in the atmosphere will increase at a rate of 7% per kelvin of surface warming. However, the climate models predict that global precipitation will increase at a much slower rate of 1 to 3% per kelvin. A recent analysis of satellite observations does not support this prediction of a muted response of precipitation to global warming. Rather, the observations suggest that precipitation and total atmospheric water have increased at about the same rate over the past two decades.

In addition to warming Earth's surface and lower troposphere, the increase in greenhouse gas (GHG) concentrations is likely to alter the planet's hydrologic cycle (*1*–*3*). If the changes in the intensity and spatial distribution of rainfall are substantial, they may pose one of the most serious risks associated with climate change. The response of the hydrologic cycle to global warming depends to a large degree on the way in which the enhanced GHGs alter the radiation balance in the troposphere. As GHG concentrations increase, the climate models predict an enhanced radiative cooling that is balanced by an increase in latent heat from precipitation (*1*, *2*). The Coupled Model Intercomparison Project (*4*) and similar modeling analyses (*1*–*3*) predict a relatively small increase in precipitation (and likewise in evaporation) at a rate of about 1 to 3% K^{-1} of surface warming. In contrast, both climate models and observations indicate that the total water vapor in the atmosphere increases by about 7% K^{-1} (*1*–*3*, *5*, *6*).

More than 99% of the total moisture in the atmosphere is in the form of water vapor. The large increase in water is due to the warmer air being able to hold more water vapor, as dictated by the Clausius-Clapeyron (C-C) relation under the condition that the relative humidity in the lower troposphere stays constant. So according to the current set of global coupled ocean-atmosphere models (GCMs), the rate of increase in precipitation will be several times lower than that for total water. This apparent inconsistency is resolved in the models by a reduction in the vapor mass flux, particularly with respect to the Walker circulation, which reinforces the trade winds (*3*, *7*). Whether a decrease in global winds is a necessary consequence of global warming is a complex question that is yet to be resolved (*8*).

Using satellite observations from the Special Sensor Microwave Imager (SSM/I), we assessed the GCMs' prediction of a muted response of rainfall and evaporation to global warming. The SSM/I is well suited for studying the global hydrologic cycle in that it simultaneously measures precipitation (P), total water vapor (V), and also surface-wind stress (τ_0), which is the principal term in the computation of evaporation (E) (*8*, *9*).

The SSM/I data set extends from 1987 to 2006. During this time Earth's surface temperature warmed by 0.19 ± 0.04 K $decade^{-1}$, according to the Global Historical Climatology Network (*10*, *11*). Satellite measurements of the lower troposphere show a similar warming of 0.20 ± 0.10 K $decade^{-1}$ (*12*). The error bars are at the 95% confidence level. This warming is consistent with 20th-century climate-model runs (*13*) and provides a reasonable, albeit short, test bed for assessing the impact of global warming on the hydrologic cycle.

When averaged globally over monthly time scales, P and E must balance except for a negligibly small storage term. This $E = P$ constraint provides a useful consistency check with which to evaluate our results. However, the constraint is valid only for global averages. Accordingly, the first step in our analysis was to construct global monthly maps of P and E at a 2.5° spatial resolution for the period 1987 to 2006.

The SSM/I retrievals used here are available only over the ocean. To supplement the SSM/I over-ocean rain retrievals, we used the land values from the Global Precipitation Climatology Project data set, which is a blend of satellite retrievals and rain gauge measurements (*14, 15*). Satellite rain retrievals over land were less accurate than their ocean counterparts, but this drawback was compensated by the fact that there are abundant rain gauges over land for constraining the satellite retrievals. Likewise, global evaporation was computed separately for oceans and land. Because 86% of the world's evaporation comes from the oceans (*16*), ocean evaporation was our primary focus. We computed evaporation over the oceans with the use of the bulk formula from the National Center for Atmospheric Research Community Atmospheric Model 3.0 (*8*, *17*). Evaporation over land cannot be derived from satellite observations, and we resorted to using a constant value of 527 mm $year^{-1}$ for all of the continents, excluding Antarctica (*16*). For Antarctica and sea ice, we used a value of 28 mm $year^{-1}$ (*8*, *16*).

The GCMs indicate that E should increase about 1 to 3% K^{-1} of surface warming. However, according to the bulk formula (eq. S1) (*8*), evaporation increases similarly to C-C as the surface temperature warms, assuming that the other terms remain constant. For example, a global increase of 1 K in the surface air temperature produces a 5.7% increase in E (*8*). To obtain the muted response of 1 to 3% K^{-1}, other variables in the bulk formula need to change with time. The air-sea temperature difference and the near-surface relative humidity are expected to remain nearly constant (*8*), and this leaves τ_0 as the one variable that can reduce evaporation to the magnitude required to balance the radiation budget in the models. To bring the bulk formula into agreement with the radiative cooling constraint, $\sqrt{\tau_0}$

Remote Sensing Systems, 438 First Street, Santa Rosa, CA 95401, USA.

*To whom correspondence should be addressed. E-mail: frank.wentz@remss.com